Heterodimeric insecticidal peptide provides new insights into the molecular and functional diversity of ant venoms

Axel Touchard[1‡], Helen C. Mendel[2‡], Isabelle Boulogne[3], Volker Herzig[2,4], Nayara Braga Emidio[2], Glenn F. King[2], Mathilde Triquigneaux[5], Lucie Jaquillard[5], Rémy Béroud[5], Michel De Waard[5,6,7], Olivier Delalande[8], Alain Dejean[1,9], Markus Muttenthaler[2,10]*, Christophe Duplais[1]*

[1]CNRS, UMR Ecofog, AgroParisTech, Cirad, INRAE, Université des Antilles, Université de Guyane, 97310 Kourou, France

[2]Institute for Molecular Bioscience, The University of Queensland, St Lucia, Queensland 4072, Australia

[3]Université de ROUEN, UFR des Sciences et Techniques, Laboratoire Glycobiologie et Matrice Extracellulaire Végétale, UPRES-EA 4358, Fédération de Recherche « Normandie Végétal » FED 4277, 76821, Mont-Saint-Aignan, France

[4]School of Science and Engineering, University of the Sunshine Coast, Sippy Downs, Queensland 4556, Australia

[5]Smartox Biotechnology, 6 rue des Platanes, 38120 Saint Egrève, France.

[6]Université de Nantes, CNRS, INSERM, L'institut du thorax, 44000 Nantes, France.

[7] LabEx «Ion Channels, Science & Therapeutics», 06560 Valbonne, France

[8]Institute of Genetics and Development of Rennes (IGDR), CNRS UMR 6290, Université de Rennes Faculté de Pharmacie, 2 avenue du Professeur Léon Bernard, 35043 Rennes, France

[9]Ecolab, Université de Toulouse, CNRS, INPT, UPS, Toulouse, France

[10]Institute of Biological Chemistry, Faculty of Chemistry, University of Vienna, 1090, Vienna, Austria

‡These authors contributed equally to this work

*Corresponding authors:

christophe.duplais@cnrs.fr, Orcid ID : 0000-0003-0926-9885

markus.muttenthaler@univie.ac.at, Orcid ID : 0000-0003-1996-4646

Abstract

Ants use venom for predation, defence and communication, however, the molecular diversity, function and potential applications of ant venom remains understudied compared to other venomous lineages such as arachnids, snakes and cone snails. In this work, we used a multidisciplinary approach that encompassed field work, proteomics, sequencing, chemical synthesis, structural analysis, molecular modelling, stability studies, and a series of *in vitro* and *in vivo* bioassays to investigate the molecular diversity of the venom of the Amazonian *Pseudomyrmex penetrator* ants. We isolated a potent insecticidal heterodimeric peptide Δ-pseudomyrmecitoxin-Pp1a (Δ-PSDTX-Pp1a) composed of a 27-residue long A-chain and a 33-residue long B-chain crosslinked by two disulfide bonds in an antiparallel orientation. We chemically synthesised Δ-PSDTX-Pp1a, its corresponding parallel AA and BB homodimers, and its monomeric chains and demonstrated that Δ-PSDTX-Pp1a had the most potent insecticidal effects in blow fly assays (LD_{50} = 3 nM). Molecular modelling and circular dichroism studies revealed strong alpha-helical features, indicating its cytotoxic effects could derive from membrane disruption, which was further supported by insect cell calcium assays. The native heterodimer was also substantially more stable against proteolytic degradation ($t_{1/2}$ =13 h) than its homodimers or monomers ($t_{1/2}$ <20 min), indicating an evolutionary advantage of the more complex structure. The proteomic analysis of *Pseudomyrmex penetrator* venom and in-depth characterisation of Δ-PSDTX-Pp1a provide novel insights in the structural complexity of ant venom, and further exemplifies how nature exploits disulfide-bond formation and dimerization to gain an evolutionary advantage *via* improved stability; a concept that is also highly relevant for the design and development of peptide therapeutics, molecular probes and bioinsecticides.

Keywords

Ant venom; Disulfide bond; Heterodimeric toxin; Cytotoxicity; Insecticide properties

Introduction

Hymenopterans are a large order of insects with ~120,000 described species and over 250 million years of evolution [1,2,3]. Many of their members, including ants, bees and wasps, use venom for predation, defence and communication. These venoms seem to be highly heterogeneous and structurally complex, with a wide range of bioactive constituents being reported including sugars, formic acid, biogenic amines, polyamines, alkaloids, and peptides [4,5]. Considering this immense chemical diversity and the high species richness of this order, hymenopterans can be considered a vast, yet understudied resource for the discovery of new biochemicals that complements venom from other, better studied species such as spiders, scorpions, snakes and cone snails. A systematic analysis of the chemical and structural diversity within hymenopteran venoms does not exist [4,5]. However, the high diversity of ant species with diverse ecology and evolutionary history predicts enormous potential for the discovery of bioactive peptides with novel structural scaffolds and pharmacology with applications in medicine and agriculture [6,7]. This potential has recently been illustrated by the discovery of a structurally unique ion channel ligand from the venom of the ant *Anochetus emarginatus* [8].

Ants belonging to the genus *Pseudomyrmex* possess venoms that rapidly subdue prey and effectively deter herbivores, suggesting that they contain both neurotoxic and cytotoxic compounds [9]. They employ their venoms according to their nesting mode (i.e., terrestrial and arboreal species, and, among the latter, plant-ants or obligate inhabitants of myrmecophytes) [10]. A previous mass spectrometry (MS)-based survey of three *Pseudomyrmex* venoms revealed that the plant-ant species *Pseudomyrmex penetrator* (*P. penetrator*) contains uncharacterized linear peptides as well as disulfide-rich peptides, indicating a complex structural diversity of toxins that warrants further investigation [11].

Here, we studied the venom of *P. penetrator* through proteomics, cytotoxicity-guided venom fractionation, chemical synthesis, structure-activity relationship (SAR) studies, proteolytic stability assays, and *in vivo* characterisation of insecticidal activity.

Results

Venom collection, mass spectrometry analysis and cytotoxicity-guided peptide isolation

A total of 11.5 mg of dried crude venom was obtained by dissecting the venom sacs from 609 *P. penetrator* workers (19 µg of dried venom *per* individual). The total amount was substantial considering the small body size of *P. penetrator* workers (~5 mm) and is linked to the relatively large size of the venom sac, which is ~0.5 mm and occupies a large volume within the ant gaster (**Fig. 1 A** and **B**).

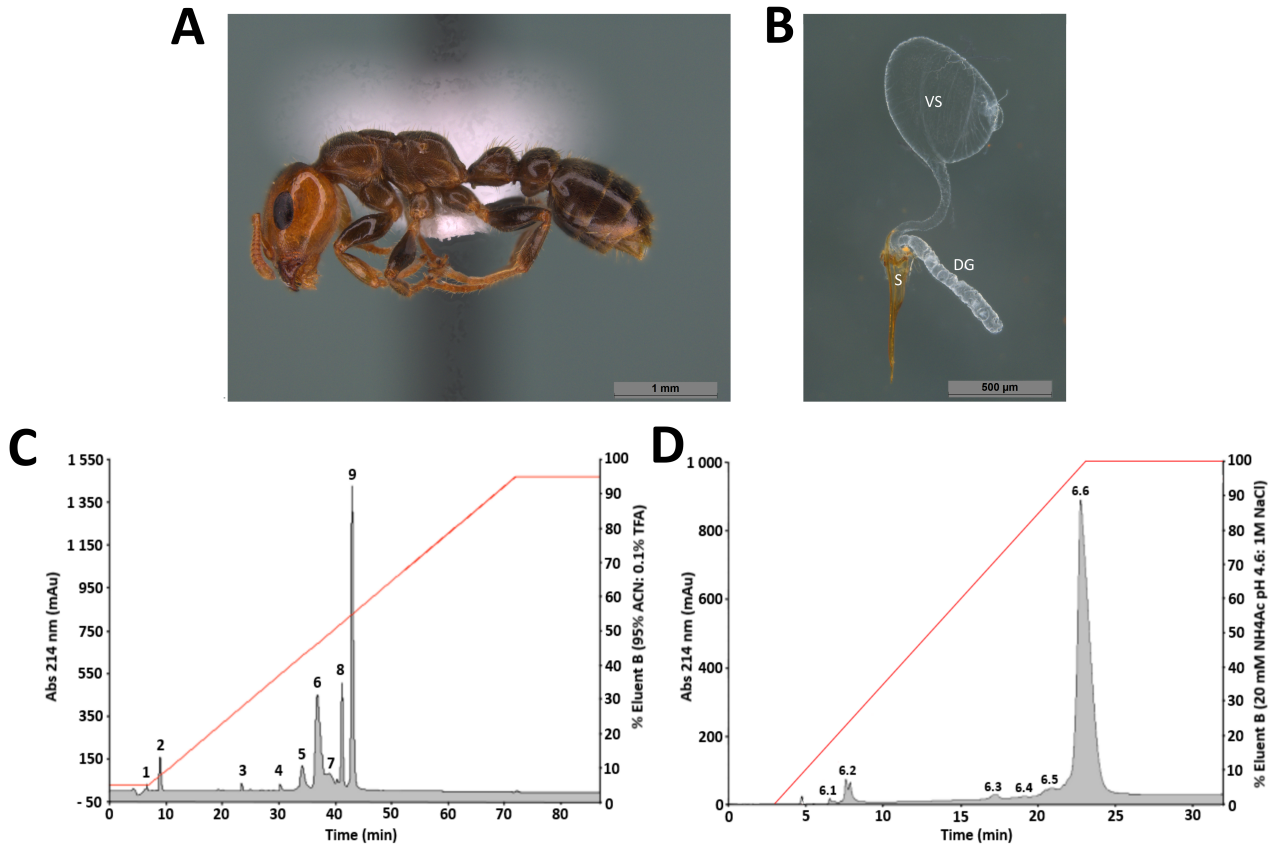

Fig. 1 Venom peptide discovery from *P. penetrator* ants. A Photo of a *P. penetrator* worker. **B** The venom sac (VS), Dufour's gland (DG) and sting (S) after dissection. **C** RP-HPLC chromatogram resulting from of *P. penetrator* crude venom fractionation on a C_{18} column. Fractions labelled from 1 to 9 were selected for cytotoxicity assays on insect cells. Fraction 6 exhibited the highest cytotoxic activity. **D** Cation-exchange chromatogram of RP-HPLC fraction 6. Sub-fractions were labelled 6.1 to 6.6. Sub-

fraction 6.6 represented > 90% of the total fraction 6 content and contained the pure cytotoxic peptide Δ-PSDTX-Pp1a.

The cytotoxicity of the crude venom was assessed by measuring growth inhibition of *Aedes albopictus* mosquito C6/36 cells. *A. albopictus* is an important vector of mosquito-borne diseases, including dengue, yellow fever, chikungunya and Zika, and its widespread geographic redistribution puts a large population at risk of contracting these diseases [12]. *A. albopictus* C6/36 cells are therefore an important *in vitro* model for the discovery of novel cytotoxic compounds and development of novel insecticidal agents. Crude *P. penetrator* venom had potent cytotoxic activity with an IC_{50} of 2 µg/mL (**Table S1**). The crude venom was then screened in a cytometry assay to examine the effects on intracellular concentrations of calcium (Ca^{2+}), sodium (Na^{+}) and chloride (Cl^{-}) ions in *A. albopictus* C6/36 cultures. Higher intracellular Ca^{2+} concentrations were observed in cells treated with *P. penetrator* crude venom (**Fig. 2**). At very low concentrations (0.03 and 0.3 µg/mL), the venom extract significantly elevated intracellular Ca^{2+} concentration (p-value <0.0001 and <0.05 respectively). No effects were observed for Na^{+} and Cl^{-} ions.

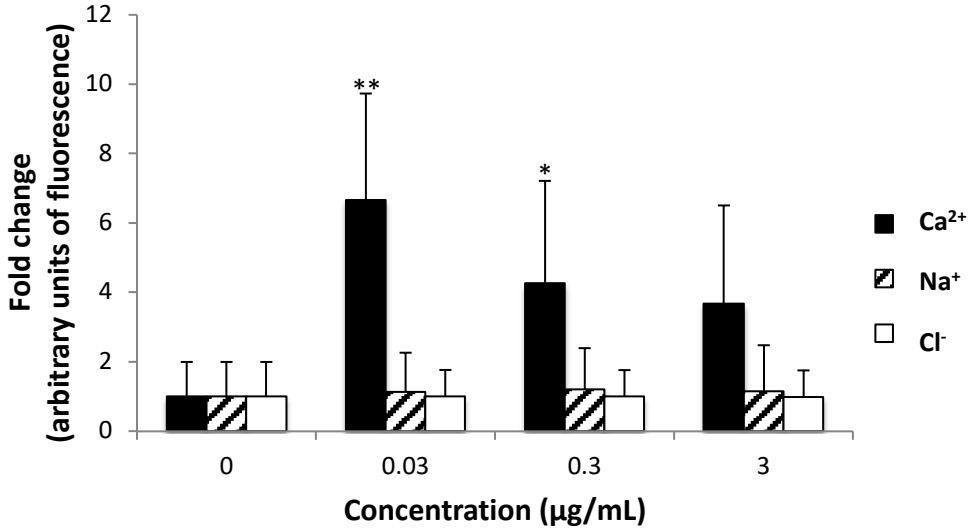

Fig. 2 Cytometry assay of crude *P. penetrator* venom. Fold change in fluorescence intensity as a proxy for intracellular Ca^{2+} (black box), Na^{+} (dashed box), Cl^{-} (white box) concentrations in *A. albopictus* C6/36 cells treated with different concentrations of crude *P. penetrator* venom. Asterisks indicate

significant differences based on non-parametric analysis using the Kruskal-Wallis test with Dunn's multiple comparison test (with ** for p-values <0.0001 and * for p-values < 0.05). Results based on four independent experiments (standard deviation error bars).

Fractionation of the crude venom using reversed-phase high-performance liquid chromatography (RP-HPLC) revealed nine peaks, with just three main (peaks 6, 8 and 9) constituting >60% of the crude venom mass (**Fig. 1C**). The monoisotopic masses of peptides in peaks 4–9 were determined by electrospray ionisation quadrupole time-of-flight mass spectroscopy (ESI-Q-TOF MS) and compared with the monoisotopic masses identified in a previous study [11] (**Table S1**). Peaks 1-3 had no defined mass and were not tested in the bioassays. A total of sixteen different peptide masses were identified ranging from 649.4–7242.1 Da including three homo- and heterodimeric peptides (5955.4, 6598.8, 7242.1 Da). Nine of the sixteen masses were previously reported [11] (**Table S1**).

The cytotoxicity of the nine RP-HPLC fractions were tested on *A. albopictus* cells (**Table S2**). Five of these fractions were cytotoxic (fractions 5 to 9). Fraction 6 was the most potent one with cytotoxic activity (IC_{50} 3.16 µg/mL) similar to the whole crude venom. Fraction 6 was further sub-fractionated by cation exchange chromatography and a heterodimeric peptide with a monoisotopic mass of 6598.8 Da was isolated (**Fig. 1D, Fig. S2**). This newly discovered ant venom peptide was highly cytotoxic to *A. albopictus* cells (IC_{50} 1.04 µM) and named Δ-pseudomyrmecitoxin-Pp1a (Δ-PSDTX-Pp1a) following established nomenclature [4]. Δ indicates peptides with cytolytic activity, PSDTX denotes peptides from ants of the subfamily Pseudomyrmecinae, 'Pp' are genus/species descriptors, and "1a" is for distinguishing paralogous peptides from the same venom [13].

Δ-PSDTX-Pp1a sequence determination, chemical synthesis and *in silico* modelling

Δ-PSDTX-Pp1a was sequenced using a combination of chemical reduction with dithiothreitol, Edman degradation, enzymatic digestion and *de novo* MS sequencing (**Table S3**). This yielded the sequence of a heterodimeric peptide comprised of a 27-residue A-chain with a C-terminal amide and a 33-residue B-chain with a C-terminal acid. Each chain contains two cysteine residues, which covalently link the two

chains through two disulfide bonds. Enzymatic degradation and MS analysis revealed an antiparallel orientation of the heterodimer with a disulfide bond connectivity of Cys_A^{I}-Cys_B^{II} and Cys_A^{II}-Cys_B^{I} (**Fig. 3**). Both peptide chains are highly cationic (predicted isoelectric point of 9.93 for A-chain and 9.70 for B-chain) and highly homologous to each other (85% sequence identity). In addition to being highly cationic (net charge of +7 for the A-chain and +6 for the B-chain) they are amphiphilic (41% and 45% hydrophobic residues, for A- and B-chain, respectively) (**Fig. S1**).

To further study Δ-PSDTX-Pp1a, we chemically synthesized this peptide *via* Fmoc-SPPS (9-fluorenymethyloxycarbonyl-solid phase peptide synthesis) in combination with a directed folding strategy using orthogonally protected cysteine building blocks with acetamidomethyl (Acm) and trityl (Trt) groups (**Fig. 3**). The first disulfide bond formation and dimerization step was carried out in a 1:1.5 ratio mixture of reduced A- and B-chains in aqueous buffer (0.5:0.75 mM A-chain:B-chain, 0.1 M NH_4HCO_3, 25°C, pH 8.3, 48 h) resulting in the expected three products, the A-B heterodimer and the two homodimers (A-A, B-B), all connected by a single bond. Following RP-HPLC purification, each product was subjected to iodine oxidation to remove the Acm group and to form the second interchain disulfide bond, thereby producing the fully folded antiparallel heterodimer and the two parallel homodimers. The synthetic heterodimer was confirmed to be identical to native Δ-PSDTX-Pp1a by a RP-HPLC coelution study and comparison of the high-resolution mass and MS fragmentation patterns (**Fig. S2**). In addition to the dimeric peptides, the single A- and B-chain were synthesized using the same Fmoc-SPPS methodology but without Acm protected cysteine residues to obtain the reduced linear A- and B-chain monomers (**Fig. S3, S4**).

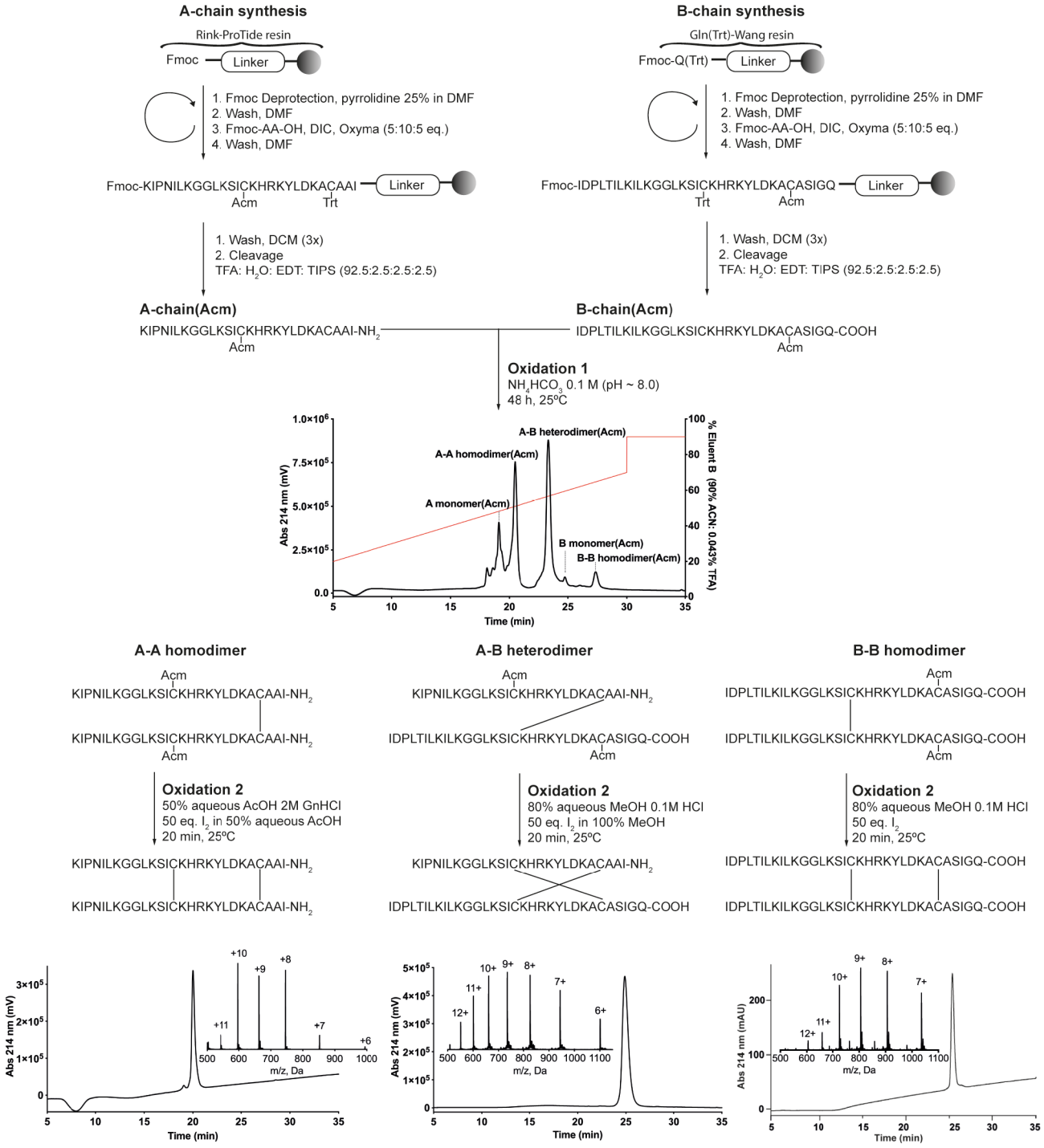

Fig. 3 Chemical synthesis of antiparallel heterodimeric Δ-PSDTX-Pp1a and the A-chain and B-chain homodimers. A-chain and B-chain peptides were assembled using Fmoc-SPPS and purified using RP-HPLC. Cysteine residues were differentially protected: A-chain Cys_A^{I} and B-chain Cys_B^{II} were protected with acetamidomethyl (Acm) and A-chain Cys_A^{II} and B-chain Cys_B^{I} with trityl (Trt). Upon treatment with trifluoroacetic acid (TFA), the peptides were deprotected and released from the resin;

Cys_A^I and Cys_B^{II} remained protected with Acm. Subsequent folding (oxidation 1) produced the single disulfide bond connected A-B heterodimer and the A-A and B-B homodimers. Acm deprotection and formation of the second interchain disulfide bond (oxidation 2) produced the fully folded A-B heterodimer and A-A and B-B parallel homodimers. After cleavage and after each oxidation, peptides were purified *via* preparative C_{18} RP-HPLC, lyophilised and analysed using analytical RP-HPLC and MS. Measured isotope peaks for the final dimer products are listed in Table S4.

To assess whether the structural or surface properties of the hetero- and homodimer peptides could affect their activity and stability, Δ-PSDTX-Pp1a and the parallel A- and B-chain homodimers were modelled *in silico* using the *de novo* PEP-fold method [14] and molecular dynamics (MD) using the Amber forcefield as implemented in Yasara [15] (**Fig. 4**). The A-chain was predicted to have a N-terminal 3_{10}-helix (Iso_A2-Lys_A7) and an α-helix (Leu_A10-Lys_A22) while the B-chain was predicted to contain two successive α-helices (Pro_B3-Gly_B12 and Leu_B14-Iso_B31) (**Fig. 4A**). The C-terminal α-helices of Δ-PSDTX-Pp1a are packed together in a compact non-coiled coil structure stabilized by two disulfide bonds (**Fig. 4B**). Most of the hydrophobic and hydrophilic residues are largely surface exposed even though the lateral chain of Asp_B25 is buried in the cationic core of the A-B heterodimer (**Fig. 4C**). This negatively charged residue likely forms a strong electrostatic interaction with the Lys_A15 and Lys_A18 of the A chain and contributes to inter-chain stability and facilitates close packing of the C-terminal α-helices. The Δ-PSDTX-Pp1a heterodimer is highly cationic with clusters of solvent-exposed Lys, Arg, His and Ser side chains, leading to an overall hydrophilic surface on one side of the heterodimer. By contrast, the other side is mostly hydrophobic except for a central hydrophilic core (**Fig. 4D**). A circular dichroism (CD) study of Δ-PSDTX-Pp1a confirmed the presence of the predicted α-helical secondary structure *via* a positive band at 190 nm and two negative bands at 208 nm and 222 nm (**Fig. 4E**).

Notably, the predicted structure of the two homodimers revealed a disordered helical conformation and a decrease of overall α-helicity in comparison to the antiparallel heterodimer (**Fig. S5** and **S6**). These disordered helical structures of both homodimers appear to be the consequence of negative interactions between similar charged residues (**Fig. S5A-D**). The BB-homodimer has similar

surface properties to Δ-PSDTX-Pp1a, albeit the hydrophobic patches are more dispersed, while the AA-homodimer has the least hydrophobic surface. Based on this structural characterization, the three dimers appear to have an amphipathic character where cationic residues represent a discontinuity within the hydrophobic patches. Therefore, it was hypothesized that the cytotoxicity activity of Δ-PSDTX-Pp1a arises from an interaction with cell membranes as often reported with such cationic amphipathic α-helical peptides [16,17].

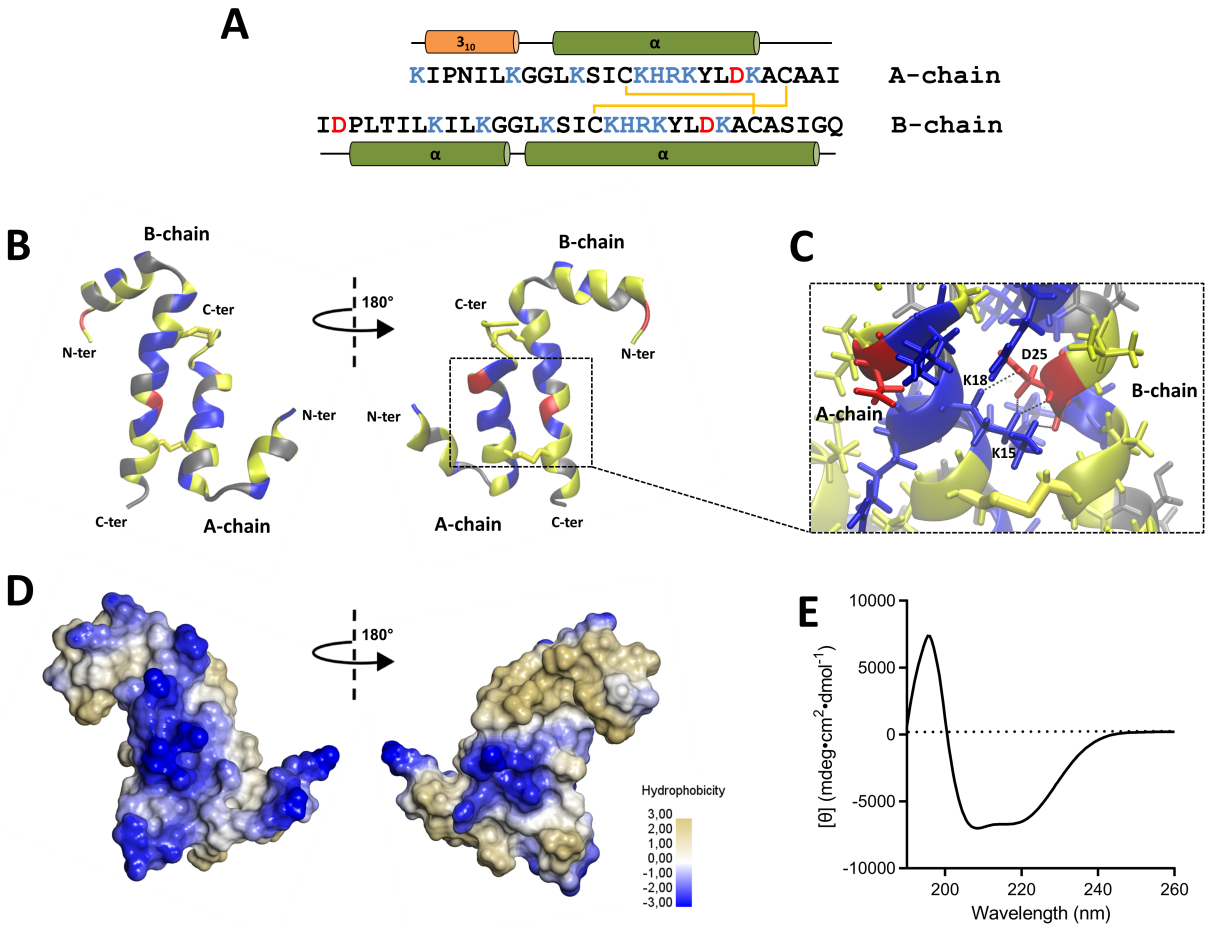

Fig. 4 Structural analysis of Δ-PSDTX-Pp1a. A Amino acid sequence of Δ-PSDTX-Pp1a with cationic and anionic residues in blue and red, respectively. Schematic representation of the predicted secondary structure of Δ-PSDTX-Pp1a is shown above and below the sequences. **B** Most representative geometry for the heterodimeric Δ-PSDTX-Pp1a peptide after clustering of a 40 ns molecular dynamics simulation. The cationic residues are in blue, anionic residues in red, polar non-charged residues in grey and hydrophobic amino acids in yellow. **C** Expanded view of the central hydrophilic core showing the buried

side chain of Asp_B25. **D** Molecular surface representation of Δ-PSDTX-Pp1a highlighting the predominance of hydrophilic patches. **E** CD spectra of Δ-PSDTX-Pp1a dissolved in sodium phosphate, pH 7.4.

Insecticidal and stability study

To gain insights into the ecological role and potential evolutionary advantage of these heterodimeric peptides, a structural class of toxins commonly reported in ant venoms, we embarked on a comparative investigation of insecticidal activity and stability of the Δ-PSDTX-Pp1a heterodimer along with the two parallel homodimers and the A- and B-chain reduced monomers. Insecticidal activity was tested *in vivo* by intrathoracic injection into sheep blowflies (*Lucilia cuprina*), a serious agricultural pest commonly used as a model organism to monitor the insecticidal activity of venom peptides [18]. The Δ-PSDTX-Pp1a heterodimer as well as the A- and B-chain homodimers exhibited the most potent insecticidal effects, with both A- and B-chain monomers being significantly less potent (**Fig. 5** and **Table S5**). For the homo- and heterodimeric peptides, contractile paralysis developed almost instantly while the flies were still attached to the injection needle and was fully developed when fly behaviour was first measured at 30 min after injection. At higher doses, paralysed flies did not recover with most being dead at 24 h post-injection.

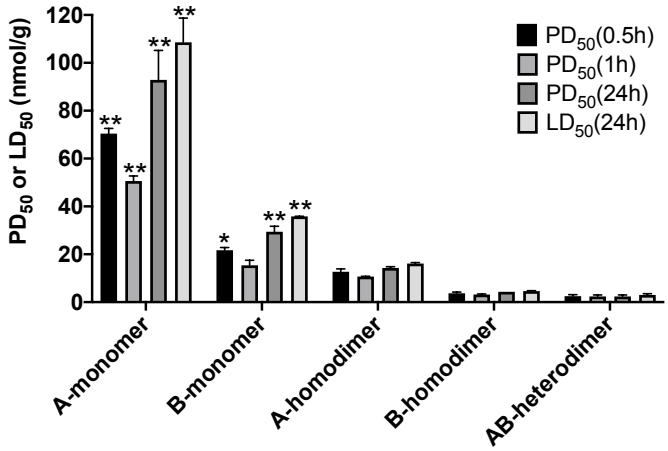

Fig. 5. **Insecticidal activity of Δ-PSDTX-Pp1a.** Paralytic and lethal effects of monomeric (A, B), homodimeric (AA, BB) and heterodimeric (AB) Δ-PSDTX-Pp1a analogues when injected into sheep

225 blowflies (*L. cuprina*). Statistical significance is based on a two-way ANOVA followed by Tukey's post
226 hoc test and indicated by * ($p<0.01$) and ** ($p<0.0001$) as compared against the respective PD_{50} and
227 LD_{50} values of the heterodimeric Δ-PSDTX-Pp1a. Error bars represent the standard error of the mean.
228
229 We then tested the proteolytic stability of the peptides by incubating them with proteinase K, a
230 broad-spectrum serine protease which cleaves peptides bonds at the C-terminal side of aromatic and
231 aliphatic residues and is used to test protein/peptide stability as it typically (37°C, pH = 7.5). Both the
232 monomers and parallel homodimers were degraded within 20 min with nearly identical kinetics. By
233 contrast, the heterodimer was exceptionally resistant to proteolytic degradation with a half-life ($t_{1/2}$) of 13
234 h, making it >39-fold more stable than the monomers and homodimers. This is particularly impressive
235 considering that the heterodimer contains 24 potential proteinase K cleavage sites dispersed throughout
236 both peptide chains (**Fig. S7**). Δ-PSDTX-Pp1a was also very stable to heat, with a stable half-life of ~13
237 h at 90°C (**Fig. S8**).

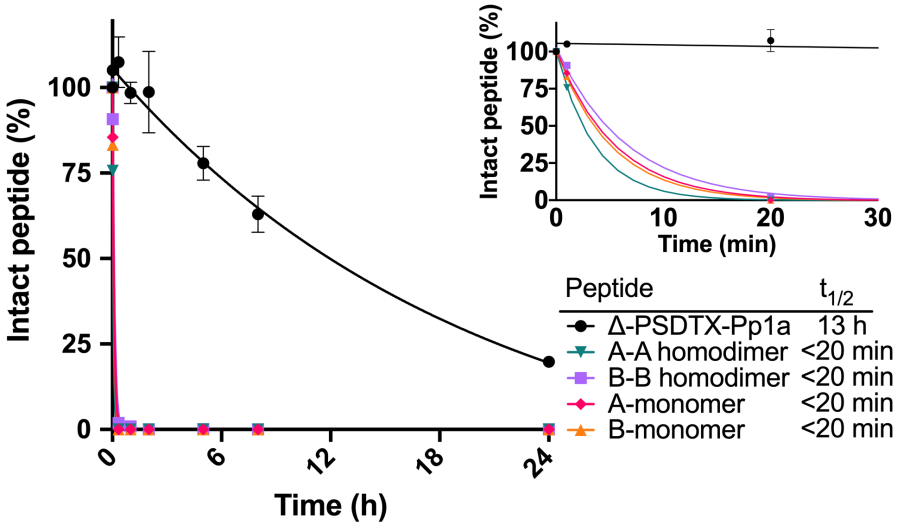

238

239 **Fig. 6 Proteolytic stability of synthetic Δ-PSDTX-Pp1a, AA-homodimer, BB-homodimer, A-**
240 **monomer and B-monomer.** Fraction of intact peptide after incubation with proteinase K (1:200
241 proteinase K:peptide molar ratio) at pH 7.5 and 37°C for up to 24 h (inset shows the first 30 min). As a
242 negative control, peptides were incubated for 24 h under the same conditions without proteinase K.
243 Peptide values were quantified relative to the negative control at t=0h. N = 2 for synthetic Δ-PSDTX-

Pp1a for A-monomer, B-monomer, and AA-homodimer, N = 1 for BB-homodimer. Experiments were performed in duplicate. Data analysis and half-life ($t_{1/2}$) calculation was performed using a non-linear fit one-phase decay model using Prism Version 8. Note the t=24 h error bars of Δ-PSDTX-Pp1a are smaller than the symbol.

Discussion

Ant species that inhabit plants (myrmecophytes) in an obligatory mutualism use a defensive venom to protect the host against defoliating insects and browsing mammals. Consequently, their venom has evolved toxins that trigger pain in vertebrates and paralyse/kill large arthropods (e.g., caterpillars, grasshoppers). Previous investigations conducted on two other plant-ant venoms (i.e., *P. triplarinus* and *Tetraponera aethiops*) revealed the presence of uncharacterized disulfide-linked dimeric peptides, suggesting that this class of toxin may have been retained in *Pseudomyrmecinae* because it participates in host plant protection [19,20]. Dimeric peptides have rarely been reported in venom peptidomes, with only a few examples in snake [21,22], scorpion [23], spider [24] and cone snail [25] venoms. Despite the fact that only a few studies have examined ant venom peptidomes, a total of 22 homo- and heterodimeric peptides have been identified from the venoms of the ant subfamilies Ectatomminae [26], Myrmeciinae [17,27], Pseudomyrmecinae [19,20] and Ponerinae [28], indicating that these structurally more complex peptides play an important role in ant venom. From an evolutionary perspective, the presence of dimeric peptides within the venom of these four ant subfamilies is also highly interesting since they constitute a non-monophyletic group [29], leading to the question on what are the evolutionary advantages of these dimeric toxins compared to monomeric toxins?

We thus set out to study the venom of *P. penetrator*, a plant-ant species that strictly uses its venom to defend the host tree [10] and revealed that the most cytotoxic component of the whole venom was Δ-PSDTX-Pp1a, a novel antiparallel heterodimer peptide. We then chemically synthesized Δ-PSDTX-Pp1a along with its homodimeric and monomeric analogues to provide an in-depth characterization of this toxin in terms of function, structure, stability and potential applications.

Insecticidal activity

Δ-PSDTX-Pp1a is a fast-acting insecticidal peptide which caused immediate paralysis when injected into blowflies leading to death within 24 h. Compared to monomeric venom peptides of other ant species, Δ-PSDTX-Pp1a with a LD_{50} (at 24 h) of 3.0 nmol/g was more lethal than the most potent insecticidal venom peptide from *Manica rubida* (LD_{50} at 24 h = 75.45 nmol/g for U_{20}-MYRTX-Mri1a, tested in *Lucilia caesar*) [30] and from *Neoponera goeldii* (LD_{50} at 24 h = 25.7 nmol/g for ponericin G1, tested in *Acheta domesticus*) [31]. To date, most of the insecticidal bioassays conducted on ant venoms revealed that the lethality of peptides is relatively weak since most exhibit non-lethal paralytic effects which are often reversible [8, 17, 30]. For instance, PONTX-Ae1a toxin isolated from the venom of the predatory ant *Anochetus emarginatus* [8] displayed similar paralytic activity to Δ-PSDTX-Pp1a on blowflies (PD_{50} at 1 h = 2.4 nmol/g for Δ-PSDTX-Pp1a and PD_{50} at 1 h = 8.9 nmol/g for PONTX-Ae1a), but this activity was completely reversible at all doses. The high lethality observed for Δ-PSDTX-Pp1a could be advantageous regarding the non-predatory behaviour of *P. penetrator* that uses its venom for long-term protection of the host-plant while predatory ants store living paralysed prey in their nest before consumption [32,33]. In a broader context, the insecticidal potency of Δ-PSDTX-Pp1a is about an order of magnitude less potent than the most spider-venom peptides that have been tested in the same blowfly toxicity assay [34,35,36].

Our structure-function relationship studies support a functional gain in lethality with dimerization, in comparison to the monomeric A- and B-chains that are only weakly active, which aligns well with a recent study on heterodimeric ant venom peptide Mp1a from *Ectatomma tuberculatum* ant [37] and a study on homotarsinin, a homodimeric peptide isolated from skin secretions of *Phyllomedusa tarsius* [38].

Stability

Δ-PSDTX-Pp1a has exceptional proteolytic and thermal stability **(Fig 6, S8)**. The proteolytic stability of the heterodimer ($t_{1/2}$ = 13 h) depends directly on its evolutionarily derived secondary structure considering that the sequence holds 24 potential proteinase K cleavage sites and that the parallel

298 homodimers were degraded 39-fold more quickly ($t_{1/2}$ < 20 min). The interplay between α-helical
299 conformation, disulfide bonds and interfacial hydrophobic interactions of dimeric peptides can be crucial
300 components for high proteolytic stability [42]. Distinctin, for example, a heterodimeric pore-forming
301 peptide found in skin secretions of the frog *Phyllomedusa distincta,* is also resistant to proteolysis [39,
302 40]. In water, distinctin forms a non-covalent four-α-helix bundle having a positively charged surface and
303 a hydrophobic core [41]. Such non-covalent structural arrangements could also be at play with Δ-
304 PSDTX-Pp1a.

305 There are several other structural features that have evolved in toxins to convey metabolic
306 stability, which is important in order to effectively reach the site of action, which is often the central
307 nervous system of animals. The inhibitor cystine knot (ICK) fold, for example, is widely found in venom
308 peptides [43] and imparts peptides with remarkable stability against proteases [44]. Another robust
309 peptide fold that imparts high protease and thermal stability is the helical arthropod-neuropeptide-
310 derived (HAND) scaffold found in some spider and centipede venoms [45]. It is now well established
311 that several ants use linear and polycationic monomeric peptides to paralyze their prey, and that these
312 peptides are generally inherently unstable and susceptible to proteolytic degradation [46,47,48].
313 Enzymatic stability is particularly important for venom peptides that have to be injected into a
314 prey/predator and find their *in vivo* target; thus, proteolytic stability could have been a natural selection
315 criterion that promoted the evolution of highly stable dimeric membrane-active peptides in ant venoms.
316

317 **Homology, function and molecular target of Δ-PSDTX-Pp1a**

318 The A and B chains of Δ-PSDTX-Pp1a have considerable sequence identity, differing only in
319 their N-terminal region (extension in B chain) or C-terminal region (extensions of 2 and 4 residues)
320 (**Fig. 7**). This high homology suggests that they are encoded by duplicated genes. Compared to other
321 dimeric venom peptides from ants, Δ-PSDTX-Pp1a chains have some sequence homology with the
322 chains of six pseudomyrmecitoxins isolated from the venom of the plant-ant species *P. triplarinus* (31–
323 36% identity and 55–59% similarity) (**Fig. 7**).
324

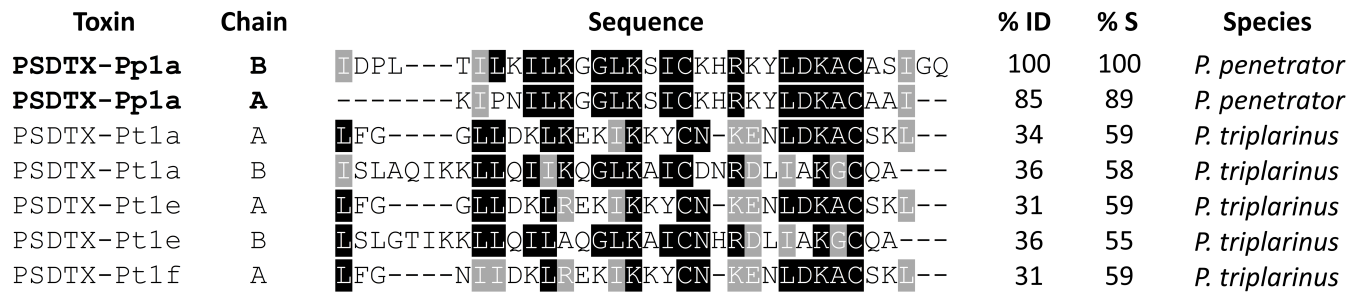

Fig. 7 Multiple sequence alignment of subunit chains belonging to dimeric pseudomyrmecitoxins. Gaps were introduced to optimise the alignment. Resulting alignments using the T-coffee alignment program were edited with BOXSHADE 3.3.1-9. Identical residues are highlighted in black while similar residues are highlighted in grey. Both percentage identity (% ID) and percentage similarity (% S) are relative to Δ-PSDTX-Pp1a chain B sequenced in this study.

These pseudomyrmecitoxins are heterodimeric polypeptides associated with the anti-inflammatory activity observed in *P. triplarinus* venom [20]. There is no significant sequence homology between Δ-PSDTX-Pp1a and the pseudomyrmecitoxins described in *T. aethiops* as for the other dimeric peptides from ant venoms. However, the predicted 3D structure of Δ-PSDTX-Pp1a aligns well with the 3D structures of two dimeric ant venom peptides, ectatotoxin Et1a (formerly ectatomin) from *Ectatomma tuberculatum* and myrmeciitoxin Mp1a (formerly pilosulin 2) from *Myrmecia pilosula* [17,49]. Indeed, despite very distinctive amino acid sequences compared to Δ-PSDTX-Pp1a, the structures of these toxins are dominated by α-helices stabilized by two or three disulfide bonds [17,49]. All of the dimeric peptides described in ant venoms share several physicochemical properties including a net positive charge (+4 to +18) due to a high lysine content, a substantial proportion of hydrophobic residues (>40%) and a mass of 5–9 kDa. These features are also shared with membrane-active peptides from ant venom that display insecticidal, cytotoxic and antimicrobial activities. Cell membranes are the common molecular target of linear, polycationic and amphiphilic ant-venom peptides [17,31,46,50]. Among ant venoms, the biological activity and the molecular target have been described for very few dimeric peptides. Nevertheless, Et1a and Mp1a, are pore-forming peptides that induce the formation of nonselective cationic channels in cell membranes, increasing cell permeability with resultant ion leakage and finally cell death [17, 51]. Similar interactions with lipid bilayers were also observed with the

348 homodimeric MIITX$_{1}$-Mg2a peptide isolated from the venom of *Myrmecia gulosa*, which produces pain
349 in vertebrates *via* the formation of pores in the membranes of peripheral sensory neurons [17]. Thus,
350 taken together, the data suggest that the cytotoxic activity of Δ-PSDTX-Pp1a is due membrane pore
351 formation.
352
353 In conclusion, Δ-Pseudomyrmecitoxin-Pp1a from the venom of *P. penetrator* is a potent cytotoxic
354 and insecticidal heterodimeric peptide that has higher potency and proteolytic stability than its
355 homodimeric and monomeric counterparts, suggesting an evolutionary advantage. This study further
356 supports that venoms of ants (Formicidae) are a promising but underexplored source of chemically
357 diverse bioactive peptides. Particularly, the presence of such structurally complex and highly stable
358 heterodimers, which seems to be more common in ant venoms than in other animal venoms, highlights
359 ant venom as an attractive biosource for interesting new ligands with applications as bioinsecticides or
360 therapeutic leads, where stability towards abiotic (pH, light, water content) and biotic (enzymes,
361 microorganisms) conditions are desired.
362
363 **Materials and Methods**
364 **Venoms collection**
365 Live *P. penetrator* workers (N = 600) were collected on La Montagne des Singes (5°04'20″N;
366 52°41'43″W) in French Guiana. We used pruning scissors to cut up *Tachigali* aff. *paniculata* compound
367 leaves containing parts of *P. penetrator* colonies and placed them in plastic bags. The boxes and plastic
368 bags containing the colonies were immediately transported to the laboratory where workers were
369 separated and sacrificed by freezing. Ant venom reservoirs were dissected and pooled in 10% v/v
370 acetonitrile (ACN)/ distilled water (v/v) (see protocol in [11]). Briefly, samples were centrifugated for
371 5 min at 12,000 *g*, then the supernatant was collected and lyophilized prior to storage at –20°C. A total
372 of 608 dissected venom sacs were used for venom fractionation, isolation and sequencing of Δ-PSDTX-
373 Pp1a as well as for the cytotoxicity assays.
374

375 **Cytotoxic bioassays**

376 *Aedes albopictus* cells C6/36 were kindly provided by the Virology Unit of the Pasteur Institute of French
377 Guiana. Each well of a 96-well plate was filled with 100 µL of insect-cell suspension (age 1 week,
378 concentration 10^5–10^7 cells/mL) and the plate was incubated for 24 h at 28°C. After incubation, the
379 supernatant was removed and replaced with 50 µL of L15 Leibovitz culture media (negative control),
380 cypermethrin (a synthetic pyrethroid) at 300, 100 and 50 µg/mL (positive controls), or venom fractions.
381 These fractions were prepared with lyophilized crude venom to obtain final concentrations of 50 to
382 0.0005 µg/mL in L15 Leibovitz culture media. Plates were incubated then for another 24 h at 28°C. After
383 incubation, 5 µL of the tetrazolium dye 3-(4,5-dimethylthiazol-2-yl)-2,5-diphenyltetrazolium bromide
384 (MTT, 5 mg/mL) was added to each well and the plate was incubated for 1 h at 28°C in darkness. The
385 supernatants were removed and 50 µL of DMSO was added to each well to suspend the formazan
386 crystals that had formed in the cells. After homogenisation by pipetting, absorbance was measured at
387 570 nm. Cytotoxic effects were determined by comparing the percentage of living cells treated with the
388 extract with the percentage of living cells treated only with the L15 Leibovitz culture media without venom
389 fractions or cypermethrin. The following formula was used: mortality rate = absorbance of the negative
390 control – (absorbance of the sample/absorbance of the negative control) ×100. Inhibition concentrations
391 (IC_{50} and IC_{99}) and their 95% confidence intervals were calculated for six technical replicates (in three
392 independent experiments) per concentration with logistic regression *via* probit analysis [52-55].
393
394 **Quantification of intracellular calcium, sodium and chloride ions**
395 Intracellular Na^+, Ca^{2+} and Cl^- concentrations were determined using the cell-permeant ion-specific
396 fluorescent dyes Corona Green Sodium Indicator, Oregon Green 488 BAPTA-1 and MQAE,
397 respectively. All assays were performed using fluorescence-activated cell sorting (FACS) and analyzed
398 with Cell Quest Pro software. Each concentration was tested using six technical replicates (in four
399 independent experiments). Each well of a 24-well plate was filled with 720 µL of *A. albopictus* cells
400 C6/36 suspension (age 1 week, concentration 10^5–10^7 cells/mL) and the plate was incubated for 24 h
401 at 28°C. After incubation, the supernatant was removed and 1 mL of the crude venom, solubilized in

L15 Leibovitz culture media, was added to obtain final concentrations of 0.03, 0.3 and 3 µg/mL. L15 Leibovitz culture media without venom was used as negative control. After 24 h at 28°C, the supernatant was removed. For Ca^{2+}, 250 µL of PBS with 63 µL of Oregon green at 40 µM was added. The plate was then incubated for 60 min at 25°C in the dark. For Cl^{-}, 500 µL of hypotonic MQAE solution at 5 mM was added. The plate was then incubated for 15 min at 37°C in the dark. For Na^{+}, 500 µL of Corona Green at 10 µM was added. The plate was then incubated for 45 min at 28°C in the dark. For all treatments, cells were washed to remove excess probes and then resuspended in 2 mL of PBS before FACS reading according to the manufacturer's instructions (Life Technologies) [56-59]. Non-parametric analyses were performed for six technical replicates (four independent experiments) per concentration using the Kruskal-Wallis test and multiple comparisons were performed with the Dunn method [49,53].

RP-HPLC fractionation and peptide purification

P. penetrator venom (11 mg) was fractionated *via* RP-HPLC using a semi-preparative-C_{18} Jupiter Proteo column (4µm, 10 x 250 mm) with a gradient comprised of solvent A [water/0.1 % (v/v) TFA] and solvent B [ACN /0.1% (v/v) TFA]. The gradient of solvent B was as follows: 5% for 7 min, 5–95% over 65 min, and 95% over 8 min at a flow rate of 3.5 mL/min. The eluate was monitored by UV absorbance at 214 nm using a diode-array detector. All analyses were performed on a Shimadzu LC-20AD system. 64 fractions of 3.5 mL were collected automatically every 1.4% of the gradient (every minute), lyophilized and stored at –20°C. Further purification of the most cytotoxic fractions was achieved by subjecting the C_{18} fractions to a second purification step using cation exchange chromatography on a TOSOH Bioscience column (TSK gel SP-STAT, 7 µm, 4.6 mm ID x 10 cm L, TOSOH Bioscience, Germany) with solvent A [200 mM sodium acetate, pH 4.6] and solvent B [200 mM sodium acetate, pH 4.6, 1 M sodium chloride]. The gradient of solvent B was as follows: 0% for 3 min, 0–100% over 20 min, and 100% over 8 min at a flow rate of 1 mL/min. The eluate was monitored by UV absorbance at 214 nm using a diode-array detector. All analyses were performed on a Shimadzu LC-20AD system. Fractions collection was based on time, every 0.5 min between 0.5 and 29.5 min (starting at 0% for 2.5 min and then the gradient itself). Major peaks were desalted by RP-HPLC using an Ascentis C_{18} column (3 µm, 4.6mm ID x 15 cm,

Sigma-Merck, Germany) using peak-based collection (slope). Sub-fractions were lyophilized for further cytotoxicity assays. The content of each HPLC fraction was analysed using MS as described in **Table S1.**

Purification and characterization of the heterodimer and sequencing

Reduction of Δ-PSDTX-Pp1a heterodimer was performed by treating 65 µg of the compound in 100 mM (50 µL) of ammonium bicarbonate buffer pH 8.5 with 40 mM tris(2-carboxyethyl)phosphine (TCEP) for 1 h at 55 ºC (volume of 50 µL), and reaction progress was monitored by MS. Monomers were then alkylated with 70 mM iodoacetamide for 1 h in the dark at 25 ºC before adding 240 mM dithiothreitol (final concentration). Finally, the sample was purified *via* RP-HPLC using an Agilent AdvanceBio peptide map column (2.1 × 250 mm) at a flow rate of 0.4 mL/min with solvent A [water/0.1% TFA (v/v)] and solvent B [ACN/0.1% TFA (v/v)]. The gradient of solvent B was as follows: 5% for 3 min, 5–15% over 1 min, 15–65% over 25 min, 95% over 4 min. The monomers were collected on Agilent 1260 HPLC (Agilent Technologies) using peak-based collection (by slope), then lyophilized. Carbamidomethyl derivates of the monomers were digested in 100 mM of ammonium bicarbonate buffer pH 8.5 with chymotrypsin or Lys-C, at a protein:enzyme ratio of 10:1, for 8 h at 37 ºC and further submitted to MS analysis.

Determination of disulfide bond connectivity

The disulfide framework of the heterodimer was determined by digesting the compound with trypsin (in 100 mM of ammonium bicarbonate buffer pH 8.5 with trypsin at a protein:enzyme ratio of 10:1) in the presence of the oxidizing reagent cystamine to narrow scrambling effects usually observed in alkaline conditions, and therefore to maintain the native configuration.

The antiparallel form, C14(PS1)-C28(PS2) and C24(PS1)-C18(PS2), was detected by MS through the detection of tryptic fragments A and B with masses of 893.4 Da and 1095.5 Da, respectively (data not shown). In contrast, the parallel configuration, C14(PS1)-C18(PS2) and C24(PS1)-C28(PS2), could be inferred from the observation of tryptic fragments C and D, 896.4 Da and 1092.5 Da, respectively.

Experimentally, Cys-containing peptides A and B were observed as predominant signals suggesting that the heterodimer was mainly in the antiparallel form with a connectivity of C14(PS1)-C28(PS2) and C24(PS1)-C18(PS2). However, the detection of fragment C by LC-MS, while minor, indicates that the parallel form may also be present. The further addition of cystamine results in an increase of the fragments A and B from the anti-parallel form in MS analyses, indicating that the parallel form could possibly result from an artefactual recombination of the disulfide bridges (data not shown). However, this cannot be concluded definitively.

Mass spectrometry

A Waters Q-TOF Xevo G2S mass spectrometer equipped with an Acquity UHPLC system and Lockspray source was used for acquisition of LC-ESI/MS and LC-ESI/MS/MS data. The dimer analysis was made by injection of 100 pmol onto the column using a 1.7 µm Acquity UPLC BEH (2.1 × 150 mm) column (Waters) at a flow rate of 0.8 mL/min with solvent A [water/0.1% formic acid (FA) (v/v)] and solvent B ACN/0.1% FA (v/v)]. The dimer was eluted using the following gradient of solvent B: 5–10% over 0.2 min, 10–70 % over 1.3 min, 70–90% over 0.1 min. Separation of monomers digests was performed using a 1.7 µm Acquity UPLC BEH300 column (Waters, 2.1 × 50 mm) at a flow rate of 0.4 mL/min with solvent A [water/0.1% FA (v/v)] and solvent B [ACN/0.1% FA (v/v)]. Injections of 150 mol of the monomer digests were made onto the column. Peptides were eluted using the following gradient of solvent B: 2% over 12 min, 2–10% over 1.2 min, 10–70% over 8 min, 70–90% over 0.6 min and 90% over 5.4 min. Mass spectrometer settings for MS analyses were a capillary voltage of 0.5 kV and a cone voltage of 40 V. The mass spectra were recorded over a scan range of 100−2000 Da. MS data were acquired using a data-dependent acquisition method (DDA) for which MS/MS data were acquired using collision energies based on mass and charge state of the candidate ions. For calibration, an external lock mass was used with a separate reference spray (LockSpray) using a solution of leucin enkephalin eluted at a flow rate of 5 µL/min. The calibration was based on the detection in MS of ions m/z 278.1141 and 556.2771 at a collision energy of 23 eV. LC/MS and LC-ESI/MS/MS data analyses were performed using MassLynx version 4.1 (Waters) software supplied by the manufacturer. The resulting MS/MS spectra data were analysed to provide *de novo* sequencing information using PEAKS® studio version 5.2 software (Bioinformatics Solutions Inc.) with the following settings: chymotrypsin or Lys-C enzyme and carbamidomethylation (C) as fixed modifications, and C-terminal amidation as variable; mass accuracy on fragment ions at 0.1 Da; mass accuracy for the precursor mass at 10 ppm. The identification of peptides was further manually validated using MS/MS spectra.

Edman degradation

Purified peptides were subjected to Edman degradation on a gas-phase sequencer model ABI 492 (Applied Biosystems, CA, USA). The phenylthiohydantoin (PTH) amino acid derivatives generated at each sequence cycle were identified and quantified on-line with an Applied Biosystems Model 140C HPLC system using the Applied Biosystems Model 610 A data analysis system for protein sequencing. The PTH-amino acid standard kit was used and reconstituted according to the manufacturer's instructions. The procedures and reagents were used as recommended by the manufacturer.

Chemical synthesis and purification of peptides

Fmoc amino acids were purchased from Iris Biotech GmbH (Marktredwitz, Germany). Fmoc-Gln(Trt)-Wang resin (loading 0.29 mmol/g) and Fmoc-Rink-ProTide resin (loading 0.19 mmol/g) were purchased from CEM Corporation (NC, USA). Fmoc-S-acetamidomethyle-L-cysteine (Fmoc-L-Cys(Acm)-OH) was purchased from Chem-Impex International. ACN was from Merck (Bayswater, Australia). *N*,*N*-dimethylformamide (DMF), TFA and diethyl ether were from Chem-Supply (Gillman, Australia). All solvents were of the highest available purity and used without further purification. All other reagents and solvents were obtained from Sigma-Aldrich (Sydney, NSW, Australia) in the highest available purity. Analytical RP-HPLC was performed on a Shimadzu LC-20AT system with a Kromasil Classic LC-MS C_{18} column (100 Å, 3.5 µm, 150 mm x 2.1 mm). Preparative HPLC was performed on a Vydac Protein and Peptide C_{18} preparative column and crude and fractions analysed using RP-HPLC (Shimadzu LC-20AT system) and ESI-MS. Mass analysis of the final products were performed on an API Q-star Pulsar Q-TOF mass spectrometer (PE SCIEX, Canada) with a Series 1100 solvent delivery system equipped with an auto-injector (Agilent Technologies Inc., Palo Alto, CA) and a Kromasil Classic LC-MS C_{18} column (100 Å, 3.5 µm, 150 mm x 2.1 mm). Data acquisition and processing were carried out using Analyst QS software v1.1 (PE SCIEX, Canada).

The Cys(Acm) protected A- and B-chain peptides used to make synthetic Δ-PSDTX-Pp1a and the parallel A-A homodimer were assembled using Fmoc-SPPS on a CEM Liberty Prime microwave peptide synthesiser. The A-chain with its C-terminal amide was synthesized on an Fmoc-Rink-ProTide resin

(scale 0.1 mmol). The B-chain with its C-terminal acid was synthesized on a preloaded Fmoc-Gln(Trt)-Wang resin (scale 0.1 mmol). Directed disulfide-bond formation was achieved using Acm-protected cysteine building blocks, where Cys1 on the A-chain and Cys2 on the B-chain were protected with Acm. Prior to the first amino acid coupling, the Fmoc group was removed *via* treatment with 25% pyrrolidine/DMF at 105 °C for 40 s. The resin was washed with DMF (2x 4 mL). Amino acid activation and couplings were carried out in DMF using Fmoc-amino acid/carbodiimide (DIC)/Oxyma (5:10:5 equivalents of resin loading) at 105 °C for 1 min. The cycle of deprotection, washing and coupling was repeated until the full-length peptide was obtained after which the resin was washed with DCM (3x) and drained. The peptide was cleaved from the resin and the side chain protecting groups (except for Acm) were removed by treatment with 15 mL TFA: water: ethandithiol: triisopropylsilane (92.5:2.5:2.5:2.5) for 40 min at 42 °C after which the cleavage solution was drained. The crude peptide was precipitated with 30 mL cold diethyl ether, centrifuged and the supernatant discarded (repeated 3x) and redissolved in 50% ACN / 0.043% TFA in water and lyophilised. The crude peptide was purified by preparative RP-HPLC and identity confirmed using analytical RP-HPLC and ESI-Q/MS. In total, 30.1 mg A chain and 61.8 mg B chain was obtained (>90% purity) with a yield of 15% and 62%, respectively.

The Cys(Acm)-protected B chain used to make the parallel B-B homodimer was synthesized using standard Fmoc-SPPS on a Symphony (Protein Technologies Inc.) automated synthesizer using Fmoc-Gln(Trt)-Wang resin (scale 0.1 mmol). Prior to first amino acid coupling, the Fmoc group was removed *via* treatment with 30% piperidine in DMF (1 x 1.5 min and 1 x 4 min) and subsequently washed with DMF. Amino acids were coupled with 0.2 M (O-(6-Chlorobenzotriazol-1-yl)-N,N,N',N'-tetramethyluronium hexafluorophosphate (HCTU) in DMF and N,N-diisopropylethylamine (DIEA) using 5-fold excess relative to resin loading (1 x 5 min then 1 x 10 min). The cycle of deprotection, washing and coupling was repeated until the full-length peptide was obtained after which the resin was washed with DCM (3x) and drained. Peptides were cleaved off the resin and side chain protecting groups were removed by treatment with TFA: water: ethandithiol: triisopropylsilane (90:5:2.5:2.5) for 2 h at 25° C. Following removal of most of the cleavage solvent under a stream of nitrogen, the crude peptide was precipitated with 30 mL cold diethyl ether, then the precipitate was washed with cold diethyl ether,

redissolved in 50% ACN / 0.043% TFA in water, and lyophilised. The crude peptide was purified by preparative RP-HPLC and identity confirmed using analytical RP-HPLC and ESI-Q/MS. In total, 18.7 mg B chain was obtained (>90% purity) with a yield of 9%.

Oxidative folding

Cys(Acm)-protected A-chain and B-chain peptide stock were diluted to 0.5 mM in a NH_4HCO_3 0.1 M solution (pH ~ 8.0) in a 1:1.5 ratio (A-chain: B-chain) and stirred at 25 °C for 48 h to form the first disulfide bond. The reaction was monitored by analytical RP-HPLC and disulfide-bond formation confirmed by ESI-MS. Three major products were obtained: the A-B chain heterodimer, A-A homodimer and B-B homodimer, all with the Cys(Acm) protecting groups intact. The oxidative mixture was purified using preparative RP-HPLC and lyophilized.

The A-B chain heterodimer with the Cys(Acm) intact was diluted to 0.1 mM in 80% aqueous MeOH 0.1 M HCl solution to form the second disulfide bond. Fifty equivalents of I_2 dissolved in 100% MeOH was added and the solution was stirred at 25°C for 10–20 min until the reaction was complete. The B-B homodimer second disulfide bond was formed using the same method as the A-B heterodimer. The A-A homodimer with the Cys(Acm) intact was diluted to 0.1 mM in 50% aqueous AcOH 2 M GnHCl solution then 50 equivalents of I_2 dissolved in 50% aqueous AcOH was added and the solution was stirred at 25°C until the reaction was complete. The reactions were monitored by LC-MS. Once completed, 1 M ascorbic acid in water was added until the solution was clear. The solution was diluted 10 times with 0.043% TFA in water and the final peptide product was isolated by RP-HPLC, identity confirmed by MS and lyophilised. In total, 9.4 mg synthetic Δ-PSDTX-Pp1a (100% purity), 1.8 mg parallel A-A homodimer (97% purity), and 0.9 mg parallel B-B homodimer (92% purity) were obtained (**Table S7**).

Reduced linear unprotected A- and B-chain peptides were synthesized, purified and analysed using the same method as described for the Cys(Acm)-protected A- and B-chains. 3 mg linear A-chain and 5.5 mg linear B-chain were obtained (>95% purity) with yields of 1% and 6%, respectively (**Table S7**).

572 **RP-HPLC co-elution study of synthetic Δ-PSDTX-Pp1a and native Δ-PSDTX-Pp1a**

573 RP-HPLC was performed using a Shimadzu LC-20AT system and a Kromasil Classic LC-MS C_{18} column
574 (100 Å, 3.5 µm, 150 mm x 2.1 mm). Solvents for RP-HPLC consisted of 0.043% TFA/ water (solvent A)
575 and 0.043% TFA/ 90% ACN/ water (solvent B). ACN was from Merck (Bayswater, Australia). TFA was
576 from Chem-Supply (Gillman, Australia).
577 The crude venom, native Δ-PSDTX-Pp1a, and synthetic Δ-PSDTX-Pp1a were run on analytical RP-
578 HPLC using a gradient of 20–70% solvent B over 25 min, at a flow rate of 0.2 mL/min. 10 µL 1 mg/mL
579 synthetic Δ-PSDTX-Pp1a in ~15% ACN/ 0.043% TFA in water was injected. 40 µL crude venom in ~15%
580 ACN/ 0.043 % TFA in water was injected. 80 µL native Δ-PSDTX-Pp1a in ~15% ACN/ 0.043% TFA in
581 water was injected.
582
583 **Molecular modelling**
584 Molecular models were produced using the *de novo* PEP-fold method [15] through the dedicated
585 webserver (v.3.1 available at http://mobyle.rpbs.univ-paris-diderot.fr/cgi-bin/portal.py#forms::PEP-
586 FOLD3), given the peptide sequences identified by MS. All structural models were submitted to
587 molecular dynamics (MD) simulations using the Amber forcefield as implemented in Yasara [15].
588 Peptides were simulated in a neutralized explicit water solvent box, under periodic boundary conditions
589 and at a constant temperature of 25˚C. MD trajectories of 40 ns were collected at 2 ps intervals for both
590 molecular systems and the production period used for analysis was set after the MD simulation reach
591 an equilibrated state (stable root mean square deviation). Clustering analysis upon trajectories provided
592 the most representative structure later considered as the final structural models. Electrostatic potentials
593 were computed by using the APBS program [62] and hydrophobic potentials were provided by the
594 Platinum webserver (http://model.nmr.ru/platinum/,[63]).
595
596 **Circular dichroism analysis of Δ-PSDTX-Pp1a**
597 Stock peptide solutions were prepared in 50% ACN/water at 1 mM concentration. Peptide
598 concentrations for electronic circular dichroism (ECD) analysis were 50 µM in PBS buffer (pH 7.4). ECD

599 spectra were obtained on a Jasco J-810 spectropolarimeter (Easton, MD, USA). All experiments were
600 carried out using a 0.1 cm quartz cell with 250 µL sample volume at 25˚C. Spectra were acquired in in
601 far UV region (185–260 nm) using 20 nm/min scan speed, 1 nm bandwidth, and 0.5 nm data pitch with
602 5 scans averaged for each sample. Blank subtraction was performed using Spectra Management
603 Software followed by curve smoothing using the binomial method. Data were processed and displayed
604 using Prism 7 (GraphPad, La Jolla USA).
605
606 **Proteolytic and thermal stability assays**
607 Samples were analysed *via* LC-MS using an API Q-Star Pulsar mass spectrometer (SCIEX, Ontario,
608 Canada) with a Series 1100 solvent delivery system equipped with an auto-injector (Agilent
609 Technologies Inc., Palo Alto, CA) using a Kromasil Classic LC-MS C_{18} column (100 Å, 3.5 µm, 150 mm
610 x 2.1 mm). Data acquisition and processing were carried out using Analyst software v1.1 (SCIEX,
611 Canada). Solvents for RP-HPLC consisted of 0.043% TFA/ water (Solvent A) and 0.043% TFA/ 90%
612 ACN/ water (Solvent B).
613
614 **Proteolytic stability**
615 70 µL of reaction buffer (0.2 M sodium phosphate, 1 mM $CaCl_2$ pH 7.5) was preheated to 37 °C for
616 30 min. 20 µL peptide stock solution (0.5 mM peptide in solvent A) and 10 µL proteinase K stock solution
617 (5 µM in reaction buffer) were added to the reaction buffer and the mixture was incubated at 37 °C for
618 24 h. Final peptide concentration was 100 µM and final proteinase K concentration was 0.5 µM (1:200
619 proteinase K:peptide molar ratio). For the negative control, 10 µL reaction buffer was added instead of
620 proteinase K. 10 µL aliquots were taken at 1 min, 20 min, 1 h, 2 h, 5 h, 8 h, and 24 h and quenched with
621 35 µL ice-cold extraction buffer (50% ACN, 0.1 M NaCl, 1% TFA) followed by centrifugation at 17,000 g
622 for 10 min. The negative control was measured at 0 h and 24 h. Samples were stored at –30°C until
623 they were analysed *via* LC-MS using a gradient of 20–90% solvent B over 25 min, at a flow rate of 0.2
624 mL/min flow. N = 2 for synthetic Δ-PSDTX-Pp1a A chain, B chain, and A-A homodimer, N = 1 for B-B
625 homodimer (due to limited amounts of peptide). Each experiment was run in duplicate with a negative

control. Peptide values were quantified relative to the negative control at 0 h and data analysis was performed using a non-linear fit one-phase decay model in Prism Version 8 (GraphPad, La Jolla USA).

Thermal stability

Δ-PSDTX-Pp1a was incubated for 72 h at 37°C, 60°C, and 90°C. 48 µL 0.05% TFA in water was preheated to 37°C, 60°C, or 90°C for 30 min. Once heated, 0.5 mM Δ-PSDTX-Pp1a was diluted in the heated buffer to a final concentration of 100 µM and a total reaction volume of 60 µL. Time points were taken at 0 h, 24 h, 48 h, and 72 h and at each timepoint 10 µL reaction solution was diluted in 35 µL 0.05% TFA in water and stored at –30°C until analysis *via* LC-MS using a gradient of 20–90% solvent B over 18 min, at a flow rate of 0.2 mL/min. Peptide values were quantified by ion extraction (ion range 1100.6–1101.6 Da) using Analyst QS 1.1 software quantification wizard. N = 3 for each peptide. Experiments were run in triplicate and samples were quantified relative to t=0 h. Data analysis was performed using a non-linear fit one-phase decay model in Prism Version 8 (GraphPad, La Jolla USA). Y0 and Plateau were constrained to 100 and 0, respectively.

***In vivo* insecticidal assays**

Insecticidal activity was evaluated injection of peptides into the ventro-lateral thoracic region of sheep blowflies (*Lucilia cuprina*; mass 22.4–31.7 mg) as previously described [60]. A 1.0 mL Terumo Insulin syringe (B-D Ultra-Fine, Terumo Medical Corporation, Maryland, USA) with a fixed 29 G needle fitted to an Arnold hand micro-applicator (Burkard Manufacturing Co. Ltd., England) was used for injection with a maximum volume of 2 µL per fly. All flies were individually housed in 2 mL tubes and paralytic activity and lethality were determined at 0.5, 1 and 24 h post-injection. A total of three tests were performed with 4–6 doses per peptide (n = 10 flies per dose) and the corresponding controls (MilliQ water; n = 10–40 per peptide). PD_{50} and LD_{50} values were calculated as previously described [64]. Two-way ANOVA with Tukey's multiple post hoc test was performed in Prism 8 for statistical comparison of the insecticidal activity of different peptides. PD_{50} and LD_{50} values for the A- and B-chain monomers and homodimers were compared to the values of the heterodimeric Δ-PSDTX-Pp1a (* $p<0.01$; ** $p<0.0001$).

Acknowledgments

This work was supported by Investissement d'Avenir of the Agence National de la Recherche (CEBA: ANR-10-LABX-25-01). We are grateful to the Virology Unit and the Medical Entomology Unit of the Pasteur Institute of French Guiana for kindly providing *Aedes albopictus* cells and *Aedes aegypti* eggs and we like to thank Geoff Brown (Department of Agriculture and Fisheries, Queensland, Australia) for the supply of blowflies. M.M. was supported by the European Research Council under the European Union's Horizon 2020 research and innovation program (714366), by the Australian Research Council (DP190101667), and by the Vienna Science and Technology Fund (WWTF; LS18-053). G.F.K. was supported by a Principal Research Fellowship (APP1136889) from the Australian National Health & Medical Research Council.

Author contributions

A.T., A.D., M.M. and C.D. conceived the study. A.T. collected and dissected ants. I.B. performed the cytotoxic and fluorometry bioassays. The peptide purification and MALDI-TOF MS/MS analysis was made by M.T., L.J. and data were analysed by L.J., M.D.W, R.B. and AT. Insecticidal assays were conducted by V. H. H.M. synthesized, purified synthetic peptides and performed the stability tests under the supervision of M.M. ECD spectra were generated by N.B.E. Structural modelling was performed by O.D and A.T. optimized the visualization. All authors discussed the results and contributed to the final manuscript.

Conflicts of interest

The authors declare no competing financial and non-financial competing interests.

679 **References**

680 1. Mayhew PJ (2007) Why are there so many insect species? Perspectives from fossils and phylogenies.
681 Biol. Rev. 82:425–454. https://doi.org/10.1111/j.1469-185X.2007.00018.x

682 2. Van Emden, H.F. Subclass pterygota, division endopterygota, order Hymenoptera (Sawflies, Ants,
683 Bees and Wasps) 120,000 described species. In Handbook of Agricultural Entomology; John Wiley &
684 Sons: Oxford, UK, 2013; pp. 193–220.

685 3. Peters RS, Krogmann L, Mayer C, Donath A, Meusemann K, Kozlov A, Podsiadlowski L, Petersen
686 M, Lanfear R, Diez PA, Heraty J, Kjer KM, Klopfstein S, Meier R, Polidori C, Schmitt T, Liu S, Zhou X,
687 Wappler T, Rust J, Misof B, Niehuis O (2017) Evolutionary History of the Hymenoptera. Curr. Biol.
688 27:1013–1018. https://doi.org/10.1016/j.cub.2017.01.027

689 4. Touchard A. Aili SR, Fox EGP, Escoubas P, Orivel, J, Nicholson, G.M.; Dejean, A. The biochemical
690 toxin arsenal from ant venoms. *Toxins* **2016**, *8*, 30.

691 5. dos Santos-Pinto, J. R. A., Perez-Riverol, A., Lasa, A. M., & Palma, M. S. (2018). Diversity of peptidic
692 and proteinaceous toxins from social Hymenoptera venoms. *Toxicon*, *148*, 172-196.
693

694 6. Aili, S.R..; Touchard, A.; Escoubas, P.; Padula, M.P.; Orivel, J.; Dejean, A.; Nicholson, G.M.; Diversity
695 of peptide toxins from stinging ant venoms. *Toxicon* **2016**, *92*, 166–178.
696

697 7. Touchard, A.; Koh, J. M. S.; Aili, S. R.; Dejean, A.; Nicholson, G. M.; Orivel, J.; Escoubas, P., The
698 complexity and structural diversity of ant venom peptidomes is revealed by mass spectrometry profiling.
699 *Rapid Commun Mass Spectrum* **2015**, 29, 385-396.
700

701 8. Touchard, A.; Brust, A.; Cardoso, F. C.; Chin, Y. K. Y.; Herzig, V.; Jin, A.-H.; Dejean, A.; Alewood, P.
702 F.; King, G. F.; Orivel, J.; Escoubas, P., Isolation and characterization of a structurally unique β-hairpin

703 venom peptide from the predatory ant *Anochetus emarginatus*. *Biochim Biophys Acta – General*
704 *Subjects* **2016,** *1860* (11, Part A), 2553-2562.
705
706 9. Sanchez, A.; Bellota, E. Protection against herbivory in the mutualism between *Pseudomyrmex*
707 *dendroicus* (Formicidae) and *Triplaris americana* (Polygonaceae). *J. Hymenopt. Res.* **2015**, *46*, 71–83.
708
709 10. Dejean, A.; Labrière, N.; Touchard, A.; Petitclerc, F.; Roux, O. Nesting habits shape feeding
710 preferences and predatory behavior in an ant genus. *Naturwissenschaften* **2014,** *101*, 323–330.
711
712 11. Touchard, A.; Labriere, N.; Roux, O.; Petitclerc, F.; Orivel, J.; Escoubas, P.; Koh, J.M.; Nicholson,
713 G.M.; Dejean, A. Venom toxicity and composition in three *Pseudomyrmex* ant species having different
714 nesting modes. *Toxicon* **2014**, *88*, 67–76.
715
716 12. Kraemer, M.U.G.; Reiner, R.C.; Brady, O.J. *et al.* Past and future spread of the arbovirus
717 vectors *Aedes aegypti* and *Aedes albopictus*. *Nat. Microbiol.* **2019**, *4*, 854–863.
718
719 13. King, G. F.; Gentz, M. C.; Escoubas, P.; Nicholson, G. M., A rational nomenclature for naming
720 peptide toxins from spiders and other venomous animals. *Toxicon* **2008**, 52 (2), 264-276.
721
722 14. Lamiable, A.; Thévenet, P.; Rey, J.; Vavrusa, M.; Derreumaux, P.; Tufféry, P. PEP-FOLD3: faster d
723 novo structure prediction for linear peptides in solution and in complex. *Nucleic Acids Res.* **2016**, *44*,
724 W449–54.
725
726 15. Krieger, E.; Darden, T.; Nabuurs, S.B.; Finkelstein, A.; Vriend, G. Making optimal use of empirical
727 energy functions: force-field parameterization in crystal space. *Proteins* **2004**, *57*, 678–683.
728

729 16. Robinson, S. D.; Mueller, A.; Clayton, D.; Starobova, H.; Hamilton, B. R.; Payne, R. J.; Vetter, I.;
730 King, G. F.; Undheim, E. A. A comprehensive portrait of the venom of the giant red bull ant, *Myrmecia*
731 *gulosa*, reveals a hyperdiverse hymenopteran toxin gene family. *Sci. Adv.* **2018,** *4*, eaau4640.
732
733 17. Dekan, Z.; Headey, S.J.; Scanlon, M.; Baldo, B.A.; Lee, T.-Z.; Aguilar, M.-I.; Deuis, J.R.; Vetter, I.;
734 Elliott, A.G.; Amado, M.; Cooper, M.A.; Alewood, D.; Alewood, P.F. Δ-Myrtoxin-Mp1a is a helical
735 heterodimer from the venom of the Jack Jumper ant with antimicrobial, membrane disrupting and
736 nociceptive activities. *Angew. Chem. Int. Ed.* **2017**, *56*, 8495–8499.
737
738 18. Guo, S.; Herzig, V.; King, G. F. Dipteran toxicity assays for determining the oral insecticidal activity
739 of venoms and toxins. *Toxicon* **2018**, 150, 297-303.
740
741 19. Pan, J.; Hink, W.F. Isolation and characterization of myrmexins, six isoforms of venom proteins with
742 anti-inflammatory activity from the tropical ant, *Pseudomyrmex triplarinus*. *Toxicon* **2000**, *38*, 1403–
743 1413.
744
745 20. Barassé, V.; Touchard, A.; Téné, N.; Tindo, M.; Kenne, M.; Klopp, C.; Dejean, A.; Bonnafé, E.;
746 Treilhou, M. The peptide venom composition of the fierce stinging ant *Tetraponera aethiops*
747 (Formicidae: Pseudomyrmecinae). *Toxins* **2019,** *11*, 732.
748
749 21. Osipov, A.V.; Kasheverov, I.E.; Makarova, Y.V., Starkov V.G.; Vorontsova, O.V.; Ziganshin, R.;
750 Andreeva, T.V.; Serebryakova, M.V.; Benoit, A.; Hogg, R.C.; Bertrand, D.; Tsetlin, V.I.; Utkin, Y.N.
751 Naturally occurring disulfide-bound dimers of three-fingered toxins: a paradigm for biological activity
752 diversification. *J. Biol. Chem.* **2008**, *283*, 14571–14580.
753

754 22. Moiseeva, N.; Bau, R.; Swenson, S.D.; Markland, Jr., F.S.; Choe, J.Y.; Liu, Z.J.; Allaire, M. Structure
755 of acostatin, a dimeric disintegrin from Southern copperhead (*Agkistrodon contortrix contortrix*), at 1.7
756 Å resolution. *Acta Crystallogr. D. Biol. Crystallogr*. **2008**, *64*, 466–470.
757
758 23. Zamudio, F.Z.; Conde, R.; Arevalo, C.; Becerril, B.; Martin, B.M.; Valdivia, H.H.; Possani, L.D. The
759 mechanism of inhibition of ryanodine receptor channels by imperatoxin I, a heterodimeric protein from
760 the scorpion *Pandinus imperator*. *J. Biol. Chem*. **1997**, *272*, 11886–11894.
761
762 24. Santos, A.D.; Imperial, J.S.; Chaudhary, T.; Beavis, R.C.; Chait, B.T.; Hunsperger, J.P.; Olivera,
763 B.M.; Adams, M.E.; Hillyard, D.R. Heterodimeric structure of the spider toxin μ-agatoxin IA revealed by
764 precursor analysis and mass spectrometry. *J. Biol. Chem*. **1992**, *267*, 20701–20705.
765
766 25. Loughnan, M.; Nicke, A., Jones, A.; Schroeder, C.I.; Nevin, S.T.; Adams, D.J.; Alewood, P.F.; Lewis,
767 R.J. Identification of a novel class of nicotinic receptor antagonists: dimeric conotoxins VxXIIA, VxXIIB,
768 and VxXIIC from *Conus vexillum*. *J. Biol. Chem*. **2006**, *281*, 24745–24755.
769
770 26. Pluzhinikov, K.; Nol'de, D.; Tertyshnikova, S.; Sukhanov, S.; Sobol, A.; Torgov, M.; Filippov, A.;
771 Arsen'ev, A.; Grishin, E., Structure-activity study of the basic toxic component of venom from the ant
772 *Ectatomma tuberculatum*. *Bioorg Khim.* **1994,** *20*, 857–871.
773
774 27. Wanandy, T.; Gueven, N.; Davies, N. W.; Brown, S. G. A.; Wiese, M. D., Pilosulins: A review of the
775 structure and mode of action of venom peptides from an Australian ant *Myrmecia pilosula*. *Toxicon*
776 **2015,** *98*, 54–61.
777
778 28. Kazuma, K.; Masuko, K.; Konni, K.; Inagaki, H. Combined venom gland transcripotomic and
779 peptidomic analysis of the predatory ant *Odontomachus monticola*. *Toxins* **2013**, *9*, 323.
780

781 29. Moreau, C. S.; Bell, C. D.; Vila, R.; Archibald, S. B.; Pierce, N. E., Phylogeny of the ants:
782 diversification in the age of angiosperms. *Science* **2006**, 312 (5770), 101-104.
783
784 30. Touchard, A.; Aili, S. R.; Téné, N.; Barassé, V.; Klopp, C.; Dejean, A.; Kini, R. M.; Mrinalini; Coquet,
785 L.; Jouenne, T.; Lefranc, B.; Leprince, J.; Escoubas, P.; Nicholson, G. M.; Treilhou, M.; Bonnafé, E.,
786 Venom peptide repertoire of the European myrmicine ant *Manica rubida*: identification of insecticidal
787 toxins. *J. Proteome Res.* **2020,** *19* (4), 1800-1811.
788
789 31. Orivel, J.; Redeker, V.; Le Caer, J. P.; Krier, F.; Revol-Junelles, A. M.; Longeon, A.; Chaffotte, A.;
790 Dejean, A.; Rossier, J., Ponericins, new antibacterial and insecticidal peptides from the venom of the
791 ant *Pachycondyla goeldii*. *J Biol Chem* **2001**, 276 (21), 17823-9.
792
793 32. Maschwitz, U.; Hahn, M.; Schönegge, P., Paralysis of prey in ponerine ants. *Naturwissenschaften*
794 **1979**, 66 (4), 213-214.
795
796 33. Orivel, J.; Dejean, A., Comparative effect of the venoms of ants of the genus *Pachycondyla*
797 (Hymenoptera: Ponerinae). *Toxicon* **2001**, 39 (2-3), 195-201.
798
799 34. Undheim, E. A.; Grimm, L. L.; Low, C.-F.; Morgenstern, D.; Herzig, V.; Zobel-Thropp, P.; Pineda, S.
800 S.; Habib, R.; Dziemborowicz, S.; Fry, B. G., Weaponization of a hormone: convergent recruitment of
801 hyperglycemic hormone into the venom of arthropod predators. *Structure* **2015**, 23 (7), 1283-1292.
802
803 35. Bende, N. S.; Dziemborowicz, S.; Mobli, M.; Herzig, V.; Gilchrist, J.; Wagner, J.; Nicholson, G. M.;
804 King, G. F.; Bosmans, F., A distinct sodium channel voltage-sensor locus determines insect selectivity
805 of the spider toxin Dc1a. *Nat Commun* **2014**, 5, 4350-4350.
806

807 36. de Araujo, A. D.; Herzig, V.; Windley, M. J.; Dziemborowicz, S.; Mobli, M.; Nicholson, G. M.;
808 Alewood, P. F.; King, G. F., Do vicinal disulfide bridges mediate functionally important redox
809 transformations in proteins? *Antioxidants & Redox Signaling* **2013**, 19 (16), 1976-1980.
810
811 37. Nixon, S.A.; Dekan, Z.; Robinson, S.D.; Guo, S.; Vetter, I.; Kotze, A.C.; Alewood, P.F.; King, G.F.;
812 Herzig, V. It Takes Two: Dimerization Is Essential for the Broad-Spectrum Predatory and Defensive
813 Activities of the Venom Peptide Mp1a from the Jack Jumper Ant *Myrmecia*
814 *pilosula*. *Biomedicines* **2020**, 8, 185.
815
816 38. Verly, R. M.; Resende, J. M.; Junior, E. F.; De Magalhães, M. T.; Guimarães, C. F.; Munhoz, V. H.;
817 Bemquerer, M. P.; Almeida, F. C.; Santoro, M. M.; Piló-Veloso, D., Structure and membrane interactions
818 of the homodimeric antibiotic peptide homotarsinin. *Scientific reports* **2017**, 7 (1), 1-13.
819
820 39. Dalla Serra, M.; Cirioni, O.; Vitale, R. M.; Renzone, G.; Coraiola, M.; Giacometti, A.; Potrich, C.;
821 Baroni, E.; Guella, G.; Sanseverino, M.; De Luca, S.; Scalise, G.; Amodeo, P.; Scaloni, A. Structural
822 features of distinctin affecting peptide biological and biochemical properties. *Biochemistry* **2008**, 47 (30),
823 7888-7899.
824
825 40. Batista, C. V.; Scaloni, A.; Rigden, D. J.; Silva, L. R.; Rodrigues Romero, A.; Dukor, R.; Sebben, A.;
826 Talamo, F.; Bloch, C. A novel heterodimeric antimicrobial peptide from the tree-frog *Phyllomedusa*
827 *distincta*. *FEBS letters* **2001**, 494 (1-2), 85-89.
828
829 41. Raimondo, D.; Andreotti, G.; Saint, N.; Amodeo, P.; Renzone, G.; Sanseverino, M.; Zocchi, I.; Molle,
830 G.; Motta, A.; Scaloni, A., A folding-dependent mechanism of antimicrobial peptide resistance to
831 degradation unveiled by solution structure of distinctin. *Proc Natl Acad Sci USA* **2005**, 102 (18), 6309-
832 6314.
833

834 42. Chen, Y.; Yang, C.; Li, T.; Zhang, M.; Liu, Y.; Gauthier, M. A.; Zhao, Y.; Wu, C., The interplay of
835 disulfide bonds, α-helicity, and hydrophobic interactions leads to ultrahigh proteolytic stability of
836 peptides. *Biomacromolecules* **2015**, 16 (8), 2347-2355.
837
838 43. Undheim, E.A.B.; Mobli, M.; King, G.F. Toxin structures as evolutionary tools: using conserved 3D
839 folds to study the evolutionary trajectory of rapidly evolving peptides. *BioEssays* **2016**, 38, 539-548.
840
841
842 44. Herzig, V.; King, G. F., The cystine knot is responsible for the exceptional stability of the insecticidal
843 spider toxin ω-Hexatoxin-Hv1a. *Toxins* **2015**, 7 (10), 4366-4380.
844
845 45. Yang, S.; Xiao, Y.; Kang, D.; Liu, J.; Li, Y.; Undheim, E. A. B.; Klint, J. K.; Rong, M.; Lai, R.; King,
846 G. F., Discovery of a selective $Na_V1.7$ inhibitor from centipede venom with analgesic efficacy exceeding
847 morphine in rodent pain models. *Proc Natl Acad Sci USA* **2013,** *110* (43), 17534-17539.
848
849 46. Téné, N.; Bonnafé, E.; Berger, F.; Rifflet, A.; Guilhaudis, L.; Ségalas-Milazzo, I.; Pipy, B.; Coste, A.;
850 Leprince, J.; Treilhou, M., Biochemical and biophysical combined study of bicarinalin, an ant venom
851 antimicrobial peptide. *Peptides* **2016,** *79*, 103-113.
852
853 47. Kim, H.; Jang, J. H.; Kim, S. C.; Cho, J. H., De novo generation of short antimicrobial peptides with
854 enhanced stability and cell specificity. *Journal of Antimicrobial Chemotherapy* **2013**, 69 (1), 121-132.
855
856 48. Bernard J, M.; Kara, P.; Lisa Cencia, R.; Phillip W, G., Degradation of naturally occurring and
857 engineered antimicrobial peptides by proteases. *Advances in Bioscience and Biotechnology* **2011**,
858 2011.
859

860 49. Nolde, D. E.; Sobol, A. G.; Pluzhnikov, K. A.; Grishin, E. V.; Arseniev, A. S., Three-dimensional
861 structure of ectatomin from *Ectatomma tuberculatum* ant venom. *J Biomol NMR* **1995**, 5 (1), 1-13.
862
863 50. Tseng, T.-S.; Tsai, K.-C.; Chen, C., Characterizing the structure–function relationship reveals the
864 mode of action of a novel antimicrobial peptide, P1, from jumper ant *Myrmecia pilosula*. *Molecular*
865 *BioSystems* **2017**, 13 (6), 1193-1201.
866
867 51. Pluzhnikov, K.; Nosyreva, E.; Shevchenko, L.; Kokoz, Y.; Schmalz, D.; Hucho, F.; Grishin, E.
868 Analysis of ectatomin action on cell membranes. *Eur. J. Biochem.* **1999**, *262*, 501–506.
869
870 52. Carrasco-Pozo, C.; Pastene, E.; Vergara, C.; Zapata, M.; Sandoval, C.; Gotteland, M. Stimulation
871 of cytosolic and mitochondrial calcium mobilization by indomethacin in Caco-2 cells: Modulation by the
872 polyphenols quercetin, resveratrol and rutin. *Biochim. Biophys. Acta* **2012**, *1820*, 2052–2061.
873
874 53. Gieseler, A.; Schultze, A. T.; Kupsch, K.; Haroon, M. F.; Wolf, G.; Siemen, D.; Kreutzmann, P.
875 Inhibitory modulation of the mitochondrial permeability transition by minocycline. *Biochem. Pharmacol.*
876 **2009**, *77*, 888–896.
877
878 54. Vidau, C.; Brunet, J. L.; Badiou, A.; Belzunces, L. P. Phenylpyrazole insecticides induce cytotoxicity
879 by altering mechanisms involved in cellular energy supply in the human epithelial cell model Caco-2.
880 *Toxicol. in Vitro* **2009**, *23*, 589–597.
881
882 55. Wu, X.; Hong, H.; Yue, J.; Wu, Y.; Li, X.; Jiang, L.; Li, L.; Li, Q.; Gao, G.; Yang, X. Inhibitory effect
883 of small interfering RNA on dengue virus replication in mosquito cells. *Virology journal* **2010**, *7*, 270.
884

885 56. Minamino, M.; Hara, M.; Ohnishi, S.; Irie, T.; Yamashita, T.; Minato, A.; Inagaki, C. Effects of protein
886 kinase and phosphatase inhibitors on slow shortening of guinea pig cochlear outer hair cells. *Brain Res*
887 **1998**, *781*, 275–283.
888
889 57. Miyazaki, H.; Shiozaki, A.; Niisato, N.; Marunaka, Y. Physiological significance of hypotonicity-
890 induced regulatory volume decrease: reduction in intracellular Cl^- concentration acting as an
891 intracellular signaling. *Am. J. Physiol. Renal Physiol.* **2007**, *292*, F1411–F1417.
892
893 58. Wang, X. Q.; Li, Y. G.; Zhong, S.; Zhang, H.; Wang, X. Y.; Qi, P. P.; Xu, H. Oxidative injury is
894 involved in fipronil-induced G2/M phase arrest and apoptosis in *Spodoptera frugiperda* (Sf9) cell line.
895 *Pesti. Biochem. Phys.* **2013**, *105*, 122–130.
896
897 59. Meier, S. D.; Kovalchuk, Y.; Rose, C. R. Properties of the new fluorescent Na^+ indicator CoroNa
898 Green: comparison with SBFI and confocal Na^+ imaging. *J. Neurosci. Methods* **2006**, *155*, 251–259.
899
900 60. Sousa, S. R.; Wingerd, J. S.; Brust, A.; Bladen, C.; Ragnarsson, L.; Herzig, V.; Deuis, J. R.; Dutertre,
901 S.; Vetter, I.; Zamponi, G. W., Discovery and mode of action of a novel analgesic β-toxin from the African
902 spider *Ceratogyrus darlingi*. *PloS one* **2017**, 12 (9).
903
904 61. Herzig, V.; Hodgson, W. C., Neurotoxic and insecticidal properties of venom from the Australian
905 theraphosid spider *Selenotholus foelschei*. *Neurotoxicology* **2008**, 29 (3), 471-475.
906
907 62. Baker, N.A.; Sept, D.; Joseph, S.; Holst, M.J.; McCammon, J.A. Electrostatics of nanosystems:
908 application to microtubules and the ribosome. *Proc. Natl. Acad. Sci. U. S. A.* **2001**, *98*, 10037–10041.
909

910 63. Pyrkov, T.V.; Chugunov, A.O.; Krylov, N.A.; Nolde, D.E.; Efremov, R.G. PLATINUM: a web tool for
911 analysis of hydrophobic/hydrophilic organization of biomolecular complexes. *Bioinforma. Oxf. Engl.*
912 **2009**, *25*, 1201–1202.

913